J. Fluid Mech. (1978), *vol.* 89, *part* 4, *pp.* 709–722
Printed in Great Britain

Measurement of turbulence quantities in a two-stream mixing layer

By M. SAIY
Department of Mechanical Engineering, Aryamehr University, Tehran, Iran

AND S. J. PEERLESS
Department of Mechanical Engineering, Imperial College, London

(Received 18 July 1974 and in revised form 1 March 1978)

Measurements have been made of the time-mean velocity, all three fluctuating velocity components and the turbulence shear stress in the plane mixing layer produced in an open wind tunnel between two nominally parallel air streams with fairly low turbulence levels. The hot-wire measuring system is described, the evaluation equations derived and the principal results presented.

1. Introduction

Recent advances in the numerical solution of the relevant differential equations have encouraged the development of analytical models of turbulent motion which are more sophisticated than the Prandtl mixing-length hypothesis. In order to assist the establishment of these new models it is necessary to have more comprehensive and detailed knowledge of turbulent flows than has hitherto existed. The plane mixing layer provides a simple flow in which to carry out this fundamental task. This report describes experimental work carried out in this type of flow. It is an extension of the work reported in Peerless (1971).

Most of the experimental examinations of two-dimensional plane jets involving investigation of the structure of turbulent shear flow have been carried out with stationary secondary flow, e.g. Liepmann & Laufer (1947), Sunyach & Mathieu (1969), Patel (1970), Bradbury (1965) and Wygnanski & Fiedler (1970). Very few workers have investigated the two-stream configuration, principally Peerless (1971), Spencer (1970) and Miller (1968). Turbulent mixing between two streams permits variation of the velocity ratio, which is defined in this work as the ratio of the secondary flow velocity U_E to the primary flow velocity U_I (figure 1). The velocity ratio affects significantly the turbulent properties and the rate of spread of the mixing region. The results for two velocity ratios (0·43 and 0·66) are presented in this report, which describes part of a larger investigation covering a range of free-stream turbulence intensities. In the present work the free-stream turbulence intensity is approximately 0·6 % in both the primary and the secondary stream.

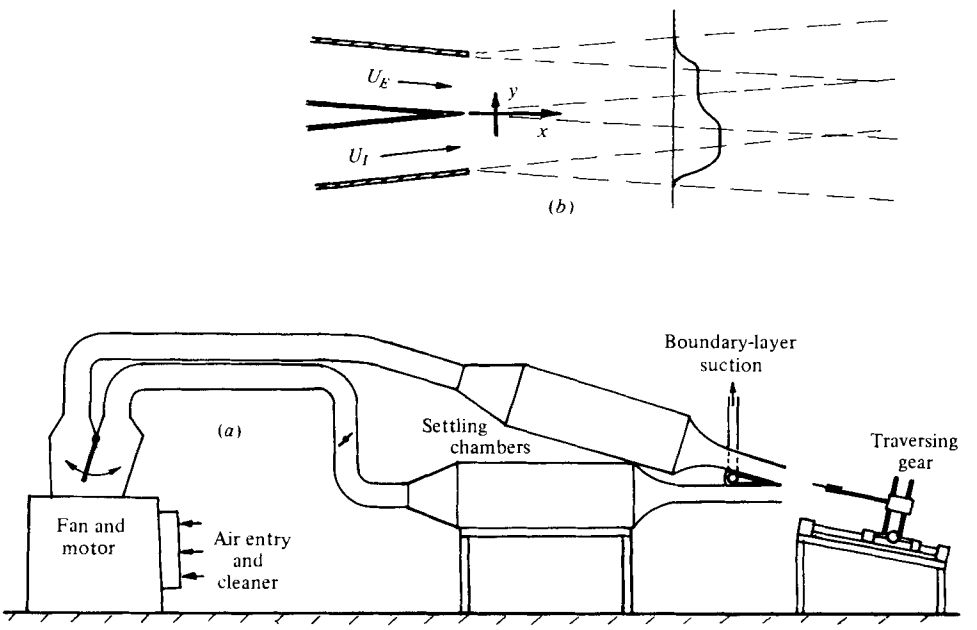

FIGURE 1. (a) Diagram of layout of apparatus. (b) Diagram illustrating growth of the central and outer mixing layers.

2. Apparatus and method

The rig in which the measurements were carried out is shown in figure 1. A centrifugal fan was used to produce the two air streams; a splitter flap at the outlet divided the flow between the two ducts so that any velocity ratio could be achieved. The fan intake was fitted with an electrostatic air filter to minimize dust contamination of the hot-wire anemometer sensors. A settling chamber was included in each duct, and in order to make the flow at the beginning of the working section more uniform, the boundary layers on the dividing wall were sucked away. To allow for the removal of the boundary-layer fluid, the dividing wall was constructed in the form of a hollow wedge with porous surfaces. The angle between the two streams of air flowing into the working section was about $8\frac{1}{2}°$.

The measuring section was open to the atmosphere at the top and bottom, but was provided with side walls to give some protection from draughts. The discharge areas of the two ducts were approximately 30 cm wide and 6 cm deep, and the velocity of the faster stream was about 25 m/s.

For calibration of the hot-wire sensors, fine control of the flow rate was provided by a butterfly valve upstream of the settling chamber in one duct.

The traversing mechanism was designed to allow movement in all three directions. The main frame slid along two steel support tubes aligned in the x direction and could be locked in any desired position. Motion in the y direction was produced by a lead screw chain-driven from a small hand-wheel. It was also possible to move the whole traversing frame in the z direction; this, however, was necessary only to check the two-dimensionality of the flow initially. A Pitot tube and hot-wire sensor were

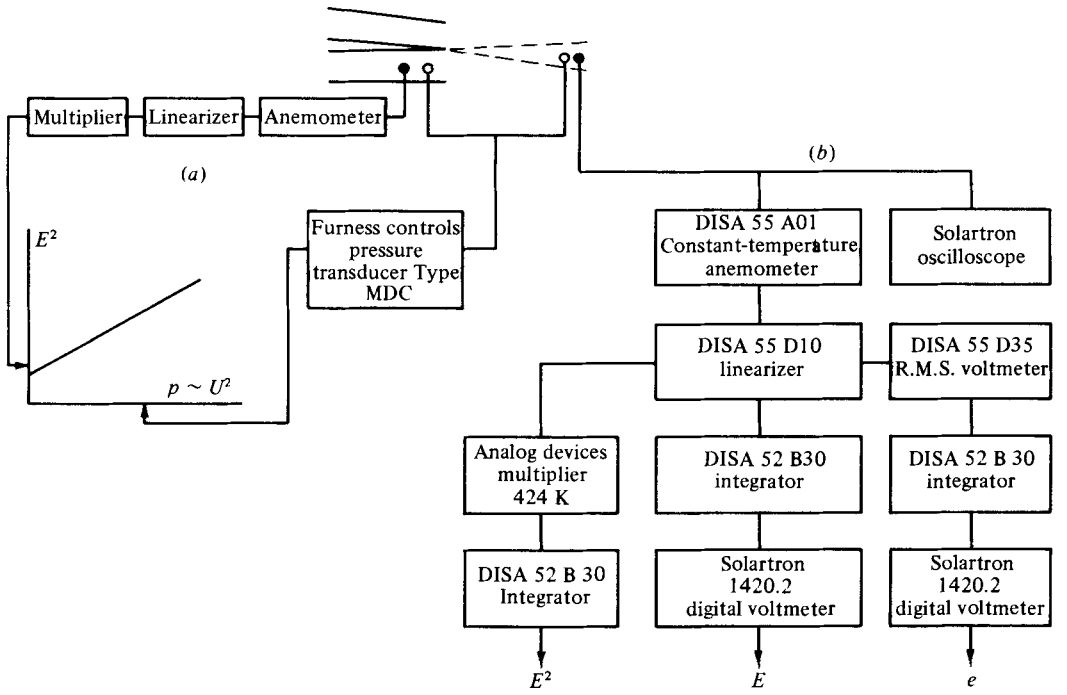

FIGURE 2. Diagram of instrumentation for (*a*) calibration of hot wire and (*b*) measurements in mixing layers. ●, hot-wire probe; ○, Pitot tube.

held at the same height and aligned with the main direction of the flow. The support of the hot wire was fixed on an indexing mechanism. This was specially made for hot wires inclined at 45° and allowed them to be set in both possible positions in both the x, y and the x, z plane.

The Pitot tube, employed for mean-velocity measurements, was a flattened stainless-steel tube with dimensions 5·8 mm and 0·38 mm in the z and y directions respectively. It had been calibrated in a separate wind tunnel against a standard NPL elliptic-profile tube and the deviation found to be 0·5 % or less. In use it was connected to a micromanometer and pressure transducer.

Two different types of hot wire were employed:

(*a*) a standard DISA 55FO1 single straight wire for u-component turbulence velocity and for the mean velocity (for comparison with Pitot-tube measurements);

(*b*) a standard DISA 55FO2 45° slanting wire for lateral turbulence velocities and Reynolds shear stresses.

Only gold-plated single probes were used. The advantage of gold-plated wires is the smaller effect of the support prongs in tangential cooling; the reason for using single-wire probes is to avoid interference between the wires.

Figure 2 shows the general form of the signal-processing equipment used. To convert the signal from the hot wires a DISA 55AO1 constant-temperature anemometer and a DISA 55D10 linearizer were employed. The linearized anemometer output $\hat{E}$ (instantaneous voltage) was fed first to a DISA 52B30 integrator to obtain the time-mean value then to a DISA 55D35 RMS-voltmeter to obtain the fluctuating part

and thus $(\overline{e^2})^{\frac{1}{2}}$. These time-mean and fluctuating components were also read on digital voltmeters. Since the linearizer cuts out all outputs larger than 10 V, the signal was monitored on an oscilloscope to make sure that no turbulence peaks were cut out. For calibration purposes the signal was also squared by means of an analog multiplier to obtain $\hat{E}^2$ ($\hat{E}^2 \approx E^2$ when $u/U < 1\,\%$, e.g. inside the duct).

All the hot wires were calibrated before use to obtain the correct exponent for the linearizer and to find the constant C in the transformation equation (A 5) (see appendix). The calibrations were carried out inside the duct, where the turbulence intensity was only about 0·5 %. The correct value of the exponent operating in the linearizer was found by trial and error so that the output signal, after being squared in the multiplier, produced a straight-line graph of E^2 *vs.* the manometer pressure p on the x, y plotter. If the calibration curve was different after the measurements for any reason, e.g. owing to dirt or a change in room temperature, the measurement was rejected.

3. Results

Figures 3 (a) and (b) show the profiles of the time-mean velocity measured by the Pitot tube at the five transverse stations (x = 10·0, 12·5, 15·0, 17·5 and 20·0 cm from the trailing edge of the dividing wall) for velocity ratios of 0·43 and 0·66 respectively. The traverses cover not only the central mixing layers, but also the greater part of each outer layer. The profiles within each layer are similar in shape, indicating that the flow is practically fully developed by the first measuring station. This is especially true of the central layer, where the boundary-layer suction on the surface of the dividing wall minimizes the size of the wake formed downstream, so that it quickly disappears in the mixing process.

All time-mean velocities were measured by a straight hot-wire probe as well as by a Pitot tube. The difference between the two measurements is small, as the typical comparison graph in figure 4 shows; this has been drawn for the central mixing layer for a single station, x = 15 cm, and a velocity ratio U_E/U_I = 0·43. The values of the velocity shown in figure 3 are those obtained from the Pitot-tube measurements.

Figure 5 (a) shows the distributions within the central mixing layer of the root-mean-square values of u, v and w, the fluctuating velocity components in the x, y and z directions, non-dimensionalized by $U_I - U_E$, for U_E/U_I = 0·43. These quantities were measured at all five stations, but for clarity the results for only three traverses (x = 10, 15 and 20 cm) are included in these graphs. The points collapse well together when plotted non-dimensionally except for the u and v components on the low-velocity side. Here the increase in the turbulence intensity with x shows the increasing effect of the outer mixing layer. In this connexion it should be appreciated that at any value of x the turbulence kinetic energy layer is significantly thicker than the velocity layer.

The turbulence-intensity distributions for U_E/U_I = 0·66 are shown in figure 5 (b). The relative intensities u/U, v/U and w/U derived directly from the hot-wire readings are, of course, lower at this higher velocity ratio. When normalized by $U_I - U_E$, however, the values are higher than those in figure 5 (a), indicating that the free-stream turbulence, although fairly low, has a larger effect on the weaker mixing layer at the higher velocity ratio. No influence of the outer mixing layers can be discerned in this case because of the smaller rate of growth of the central layer.

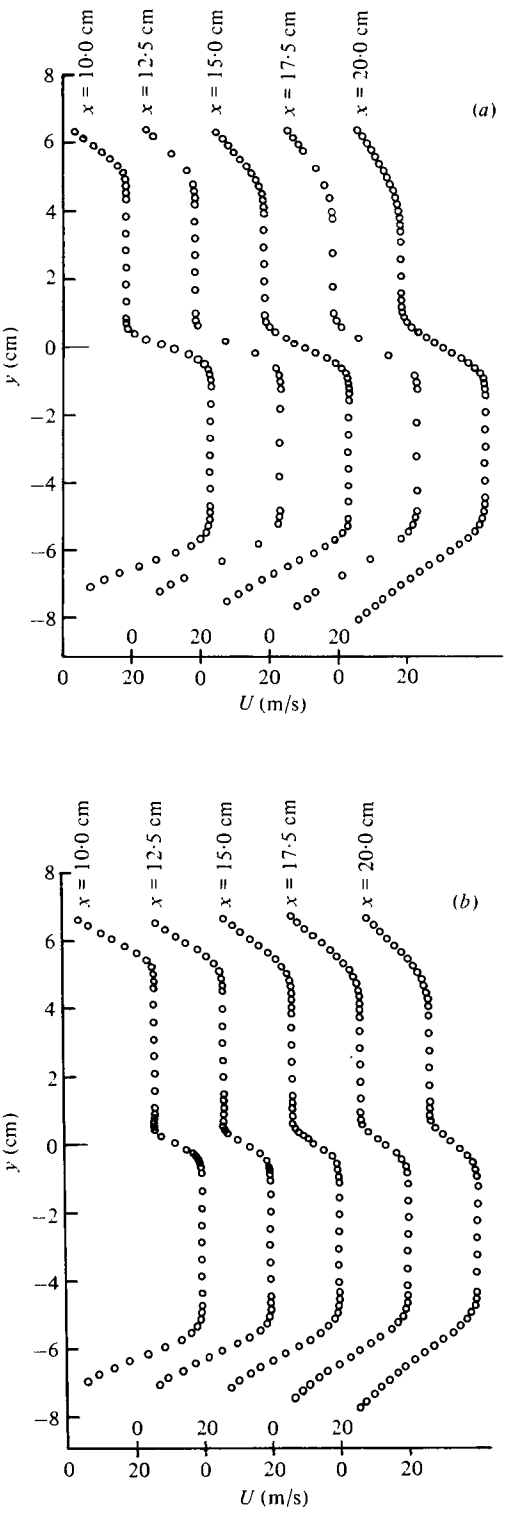

FIGURE 3. Computer plot of complete velocity profiles at $x = 10{\cdot}0$, 12·5, 15·0, 17·5 and 20·0 cm for (*a*) $U_E/U_I = 0{\cdot}43$ and (*b*) $U_E/U_I = 0{\cdot}66$.

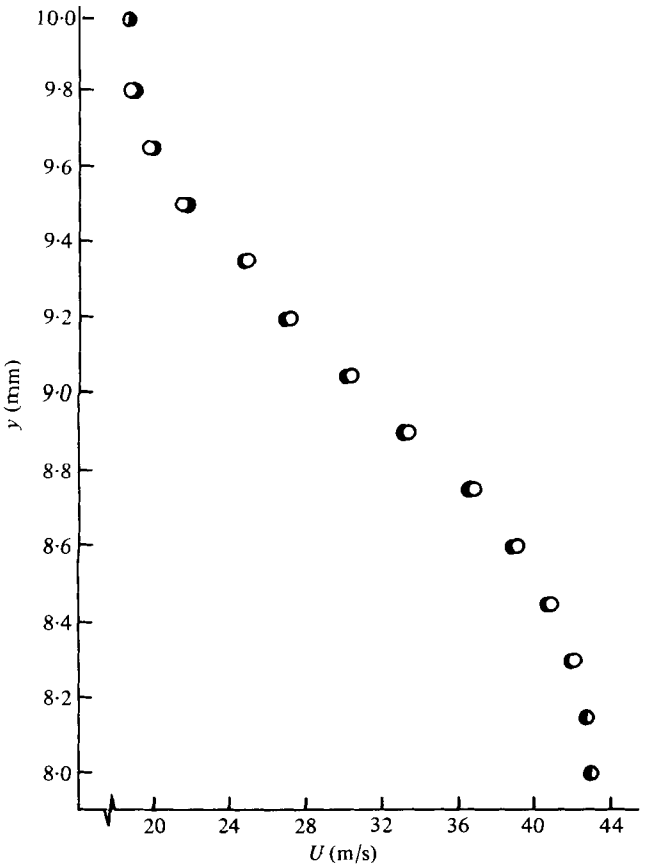

FIGURE 4. Comparison of mean velocity profiles measured with a Pitot tube and a hot wire. $U_E/U_I = 0{\cdot}43$. ○, Pitot tube; ●, hot wire.

It will be seen that for both velocity ratios the v component of the fluctuations has a smaller peak than either of the other two components. A second point of interest is that the peaks of the v-component profiles are further to the right (i.e. towards the low-speed side of the mixing layer). Note that in these graphs the vertical axis is drawn where $y^* = 0$, i.e. where the time-mean velocity U is the average of the two free-stream values U_I and U_E.

Profiles of the non-dimensional turbulence kinetic energy $\frac{1}{2}q^2$ for the two velocity ratios are shown in figure 6; again, for clarity, the results for only three transverse stations are included. Values of q^2 are obtained from the local relative turbulence intensities $[q^2 = (\overline{u}^2 + \overline{v}^2 + \overline{w}^2)/U^2]$. These graphs clearly indicate the approximately self-preserving character of the mixing layer within the zone of the measurements.

Values of the non-dimensional turbulence shear stress, obtained from equation (A 15) (see appendix), are plotted in figure 7.

The ratio $\overline{vu}/q^2$, for which Townsend (1976) uses the symbol a_1, is shown in figure 8. The distributions for the two velocity ratios are noticeably different in shape: for $U_E/U_I = 0{\cdot}43$ there is a distinct central plateau with a value of about 0·18 whereas no such plateau occurs for the higher velocity ratio and the values of a_1 are everywhere lower.

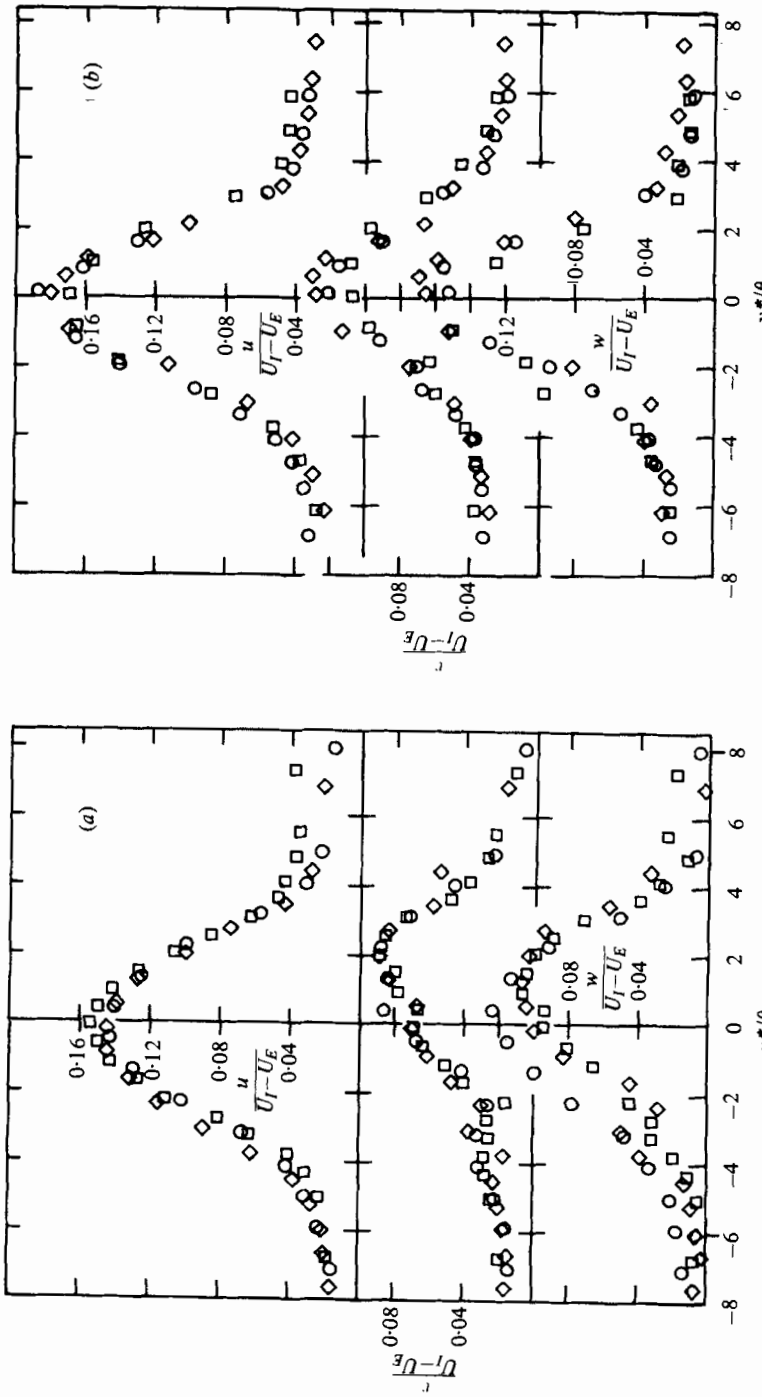

FIGURE 5. Distributions of fluctuating velocity components u, v and w for (*a*) $U_E/U_I = 0{\cdot}43$ and (*b*) $U_E/U_I = 0{\cdot}66$. ○, $x = 10{\cdot}0$ cm; ◇, $x = 15{\cdot}0$ cm; □, $x = 20{\cdot}0$ cm.

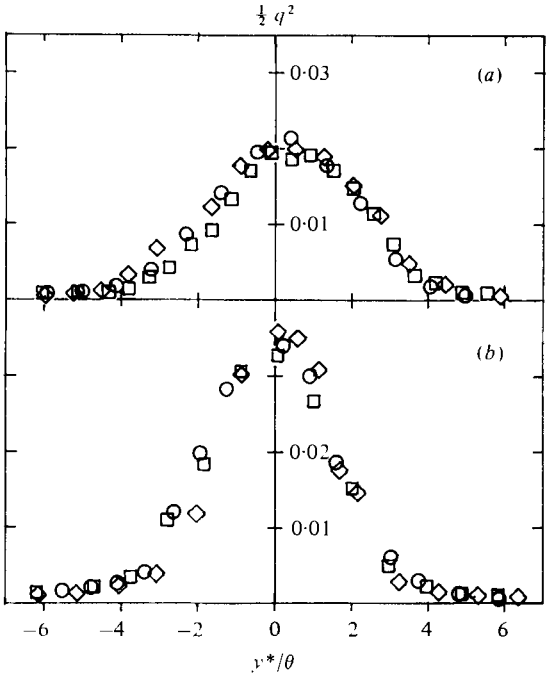

FIGURE 6. Distributions of turbulence kinetic energy for (*a*) $U_E/U_I = 0{\cdot}43$ and (*b*) $U_E/U_I = 0{\cdot}66$. ○, $x = 10{\cdot}0$ cm; ◇, $x = 15{\cdot}0$ cm; □, $x = 20{\cdot}0$ cm.

Figure 9 indicates that in a two-dimensional mixing layer the momentum thickness θ is linearly proportional to the x-wise distance. It also shows that for the lower velocity ratio the growth rate is higher. The momentum thickness has been used as an indication of the transverse width of the layer as it is less subject to random fluctuations than alternative measures of the thickness.

4. Discussion and conclusion

Experimental investigators in the field of free shear layers are frequently concerned with establishing the self-preserving character of the flows being measured. For both practical and fundamental reasons, as discussed in detail by Townsend, no real free shear flow can be exactly self-preserving. The reason most likely to have been significant in the present investigation is the inevitable x-wise variation of free-stream turbulence. Although no effect attributable to this variation is discernible in the results, and the differences between the profiles in each set are within acceptable experimental limits, nevertheless the external turbulence level of about 0·006 cannot be entirely negligible compared with the inherent levels within the mixing layer; these have peak values, for u/U, of about 0·13 and 0·065 respectively for $U_E/U_I = 0{\cdot}43$ and 0·66.

The same observation is probably true of other investigations of free shear layers in the literature, although free-stream intensities are rarely quoted. Only in the work of Peerless (1971) has serious attention been paid to the influence of free-stream turbulence on the streamwise development of the flow, although Patel (1970) has examined this effect to a limited extent. It is hoped to describe the results obtained with higher turbulence levels in a subsequent paper.

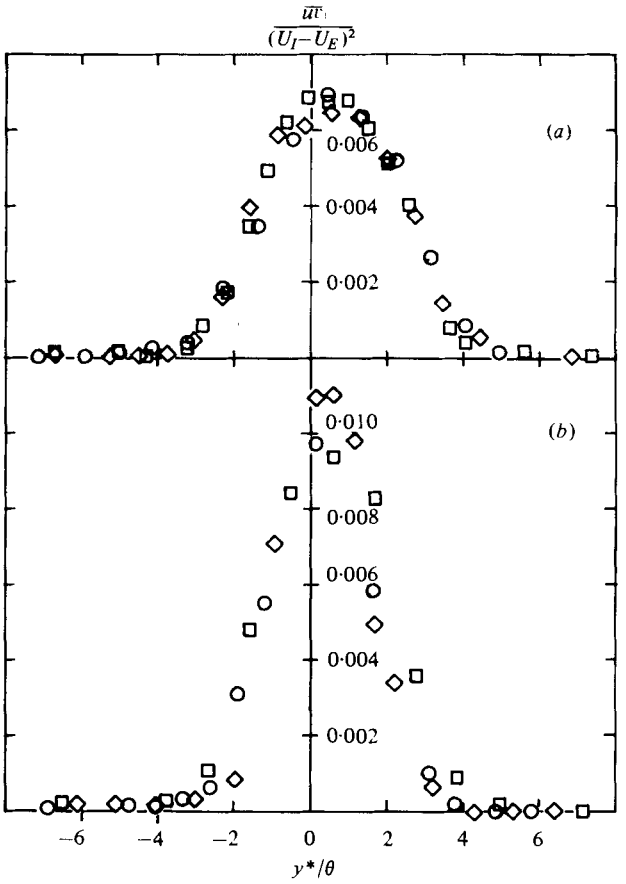

FIGURE 7. Distributions of turbulence shear stress for (*a*) $U_E/U_I = 0{\cdot}43$ and (*b*) $U_E/U_I = 0{\cdot}66$. ○, $x = 10{\cdot}0$ cm; ◇, $x = 15{\cdot}0$ cm; □, $x = 20{\cdot}0$ cm.

Comparisons with other work by Spencer (1970) and Peerless (1971) are made in figure 10. In figure 10(*a*) the peak value of the x-wise relative turbulence intensity component is plotted against the free-stream velocity ratio U_E/U_I. There is good agreement between the results from the three sources. (It should be noted here that the present work was carried out on the same apparatus as that used in Peerless (1971), after only minor modifications.)

In figure 10(*b*) the growth rates obtained from the same three sources are plotted against the velocity ratio. The agreement is again seen to be good.

The general result of the measurements is that the mixing layers examined in the present investigation are substantially self-preserving within the range of measurements and that the principal features are in good agreement with other investigations despite possible causes of discrepancy such as differences in the free-stream turbulence level, differences in the geometry of the apparatus and differences in the hot-wire technique (in particular, in the exponent in the effective cooling law used in deriving the hot-wire response equations, i.e. King's law).

In fact the only major difference between the present results and those of Spencer

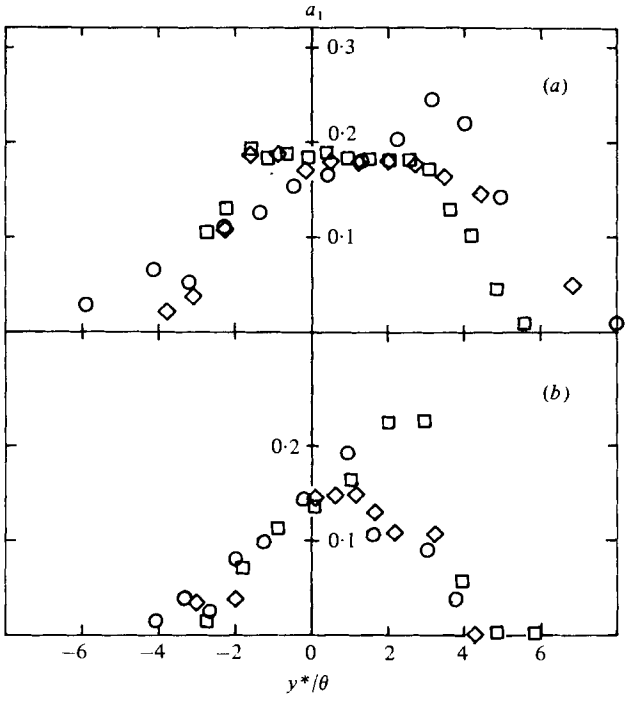

FIGURE 8. Distributions of $a_1(\equiv \overline{uv}/q^2)$ for (*a*) $U_E/U_I = 0{\cdot}43$ and (*b*) $U_E/U_I = 0{\cdot}66$. ○, $x = 10{\cdot}0$ cm; ◇, $x = 15{\cdot}0$ cm; □, $x = 20{\cdot}0$ cm.

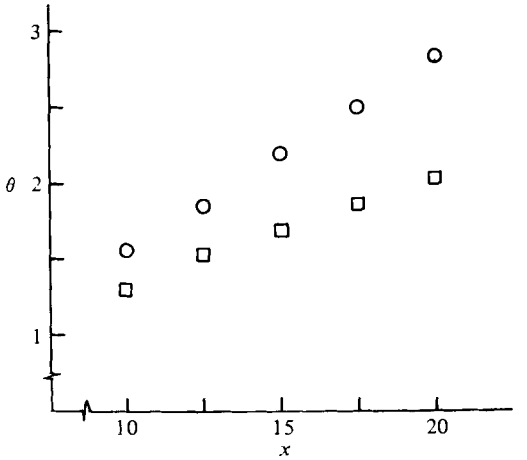

FIGURE 9. Growth of the central mixing layer. ○, $U_E/U_I = 0{\cdot}43$; □, $U_E/U_I = 0{\cdot}66$.

concerns the maximum Reynolds stress occurring in the mixing layer. For

$$U_E/U_I = 0{\cdot}66$$

the difference is less than 10 %, but for a velocity ratio of 0·44 the difference is about 25 %, the present results being lower.

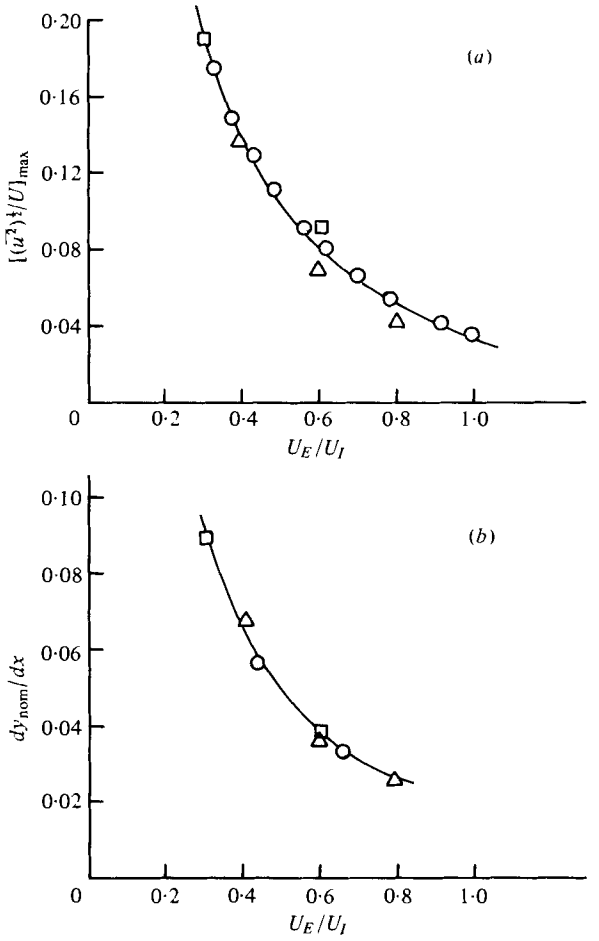

FIGURE 10. Comparison of results from different sources. △, Peerless (1971), $x = 15$ cm; □, Spencer (1970), $x = 22$ cm; ○, present work, $x = 15$ cm. y_{nom} = width of mixing layer between points for which $(U - U_E)/(U - U_E) = 0{\cdot}1$ and 0·9.

The authors thank the Ministry of Defence (Procurement Executive) for supporting the work described in this paper and for permission to publish the results.

Appendix. Response equations for single hot-wire sensors

To evaluate the response of an inclined hot wire one can assume either the simple cosine law, i.e.

$$U_{\text{eff}} = \hat{U}\cos\beta,$$

which relates the effective cooling velocity U_{eff} to the actual instantaneous fluid velocity $\hat{U}$, β being the angle between the direction of $\hat{U}$ and the perpendicular to the wire (as shown in figure 11), or a more complete form taking the effect of the tangential cooling velocity into account, e.g. the proposal of Champagne & Sleicher (1967). The tangential cooling effect varies with the length-to-diameter ratio of the sensor because of the influence of the probe supports on the flow around the wire. For sensors of high

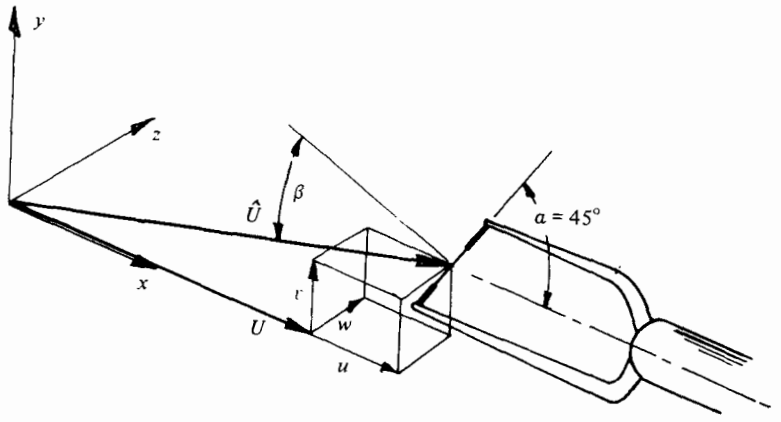

FIGURE 11

length-to-diameter ratio, say of the order of 300 upwards, the cosine cooling law given above is appropriate. In this work however, the method of Champagne & Sleicher is used, a hot wire in a turbulent field being assumed to obey the relation

$$U_{\text{eff}}^2 = \hat{U}^2(\cos^2\beta + K^2\sin^2\beta), \tag{A 1}$$

where K is a constant considerably less than unity.

$\hat{U}$, the instantaneous velocity, can be expressed as

$$\hat{U} = [(U+u)^2 + v^2 + w^2]^{\frac{1}{2}}, \tag{A 2}$$

where u, v and w are the instantaneous values of the velocity fluctuations in the x, y and z directions respectively.

From these equations, Champagne & Sleicher (1967) have derived the expression

$$\begin{aligned} U_{\text{eff}}^2 = U^2\cos^2\alpha\Bigg[1 + 2\frac{u}{U} + \frac{u^2-v^2}{U^2} + \frac{1}{\cos^2\alpha}\left(\frac{u^2+v^2}{U^2}\right) \\ + 2\tan\alpha\left(\frac{v}{U} + \frac{\overline{vu}}{U^2}\right) + K^2\Bigg\{\frac{w^2+2v^2}{U^2} - \frac{1}{\cos^2\alpha}\left(\frac{w^2+v^2}{U^2}\right) \\ - 2\tan\alpha\left(\frac{v}{U} + \frac{\overline{vu}}{U^2}\right) + \tan^2\alpha\left(1 + 2\frac{u}{U} + \frac{u^2+v^2+w^2}{U^2}\right)\Bigg\}\Bigg]. \end{aligned} \tag{A 3}$$

After some manipulation this gives

$$\begin{aligned} U_{\text{eff}}^2 = U^2\cos^2\alpha\Bigg[1 + K^2\tan^2\alpha + 2(1+K^2\tan^2\alpha)\frac{u}{U} + 2(1-K^2)\tan\alpha\frac{v}{U} \\ + (1+K^2\tan^2\alpha)\frac{u^2}{U^2} + (K^2+\tan^2\alpha)\frac{v^2}{U^2} + \frac{1}{\cos^2\alpha}\frac{w^2}{U^2} + 2\tan\alpha(1-K^2)\frac{vu}{U^2}\Bigg]. \end{aligned} \tag{A 4}$$

Now

$$\hat{E}^2 = C \times U_{\text{eff}}^2, \tag{A 5}$$

where C is a constant, and $\hat{E}$, the instantaneous voltage, can be separated into the time-mean component E and a fluctuating part e, thus

$$(E+e)^2 = C \times U_{\text{eff}}^2, \tag{A 6}$$

$$E^2 + 2Ee = C \times U_{\text{eff}}^2, \tag{A 7}$$

e^2 being neglected since the turbulence level is low. Inserting (A 4) in (A 7) for a zero turbulence level gives

$$E^2 = U^2 \cos^2\alpha[1 + K^2 \tan^2\alpha]. \tag{A 8}$$

From (A 7) and (A 8),

$$\frac{E^2 + 2Ee}{E^2} = \frac{U_{\text{eff}}^2}{U^2 \cos^2\alpha[1 + K^2 \tan^2\alpha]}. \tag{A 9}$$

Use of the expression (A 4) for U_{eff} and some manipulation then gives

$$\frac{e}{E} = \frac{u}{U} + \frac{(1-K^2)\tan\alpha}{(1+K^2\tan^2\alpha)}\frac{v}{U^2} + \frac{1}{2}\frac{v^2}{U^2} + \frac{K^2+\tan^2\alpha}{2(1+K^2\tan^2\alpha)}\frac{v^2}{U^2} + \frac{1}{2\cos^2\alpha(1+K^2\tan^2\alpha)}\frac{w^2}{U^2} + \frac{\tan\alpha\,(1+K^2)}{(1+K^2\tan^2\alpha)}\frac{\overline{uv}}{U^2}. \tag{A 10}$$

Squaring, taking the time mean and eliminating terms of order higher than $(u/U)^2$, we finally have

$$\frac{\overline{e^2}}{E^2} = \frac{\overline{u^2}}{U^2} + \left[\frac{(1-K^2)\tan\alpha}{1+K^2\tan^2\alpha}\right]^2 \frac{\overline{v^2}}{U^2} + \frac{2(1-K^2)\tan\alpha}{(1+K^2\tan^2\alpha)}\frac{\overline{uv}}{U^2}, \tag{A 11}$$

which has also been derived by Durst (1971).

The following evaluation equations can be obtained from (A 11).

(*a*) For $\alpha = 0$ (straight wire perpendicular to the direction of the time-mean velocity),

$$\overline{u^2}/U^2 = (\overline{e^2}/E^2)_{\alpha=0}. \tag{A 12}$$

(*b*) In the x, y plane, for $\alpha = \pm 45°$,

$$\frac{\overline{v^2}}{U^2} = \frac{1}{2}\left(\frac{1+K^2}{1-K^2}\right)\left[\left(\frac{\overline{e^2}}{E^2}\right)_{\alpha=+45°} + \left(\frac{\overline{e^2}}{E^2}\right)_{\alpha=-45°} - 2\left(\frac{\overline{e^2}}{E}\right)_{\alpha=0}\right]. \tag{A 13}$$

(*c*) In the x, z plane, for $\alpha = \pm 45°$,

$$\frac{\overline{w^2}}{U^2} = \frac{1}{2}\left(\frac{1+K^2}{1-K^2}\right)\left[\left(\frac{\overline{e^2}}{E^2}\right)_{\alpha=+45°} + \left(\frac{\overline{e^2}}{E^2}\right)_{\alpha=-45°} - 2\left(\frac{\overline{e^2}}{E}\right)_{\alpha=0}\right]. \tag{A 14}$$

(*d*) To obtain the turbulence shear stress, the hot wire must be in the x, y plane as in case (*b*) but one has to subtract the two equations obtained from the signals for $\alpha = \pm 45°$, thus

$$\frac{\overline{uv}}{U^2} = \frac{1+K^2}{4(1-K^2)}\left[\left(\frac{\overline{e^2}}{E^2}\right)_{\alpha=45°} - \left(\frac{\overline{e^2}}{E^2}\right)_{\alpha=-45°}\right]. \tag{A 15}$$

Equations (A 12)–(A 15) were used to analyse the hot-wire signals.

Application of the equations

In practice all the values for $e_{\alpha=0}$ are obtained in the usual way with a straight wire aligned in the z direction. This avoids errors arising from measurement with a wire aligned in the y direction (as implied by the analysis) in a stream with significant velocity gradients in that direction.

Since we are here concerned with plane two-dimensional flow, wires inclined at $\pm 45°$ in the x, z plane will give identical signals.

There is somewhat conflicting evidence about the correct value of the coefficient K. Durão (1971) indicates a value of about 0·15 for wires inclined at $\alpha = 45°$ while Rodi (1971) suggests lower values, both being concerned with gold-plated probes of the kind used in the present investigation. The value of K used in processing the results shown here was 0·1.

REFERENCES

BRADBURY, L. J. S. 1965 The structure of a self-preserving turbulent plane jet. *J. Fluid Mech.* **23**, 31.

CHAMPAGNE, F. H. & SLEICHER, C. A. 1967 Turbulence measurements with inclined hot-wires. *J. Fluid Mech.* **28**, 153.

DURÃO, D. F. G. 1971 Turbulent mixing of co-axial jets. M.Sc. thesis, University of London.

DURST, F. 1971 The application of hot-wire anemometers in low and highly turbulent flows. *TECHNICA* no. 409, Ano XLVI, vol. XXXIII.

LIEPMAN, H. W. & LAUFER, J. 1947 Investigation of free turbulent mixing. *N.A.C.A. Tech. Note* no. 1257.

MILLER, R. D. 1968 Numerical and experimental investigations of the shear layer between two parallel streams. *J. Fluid Mech.* **33**, 591.

PATEL, R. P. 1970 A study of two-dimensional symmetric and asymmetric turbulent shear flows. Ph.D. thesis, Dept. Mechanical Engineering, McGill University.

PEERLESS, S. J. 1971 Ph.D. thesis, Faculty of Engineering, London University.

RODI, W. 1971 A new method of analysing hot-wire signals in highly turbulent flow and its evaluation in a round jet. *Mech. Engng Dept., Imp. Coll., Rep.* ET/BN/B/10.

SPENCER, B. W. 1970 Statistical investigation of turbulent velocity and pressure fields in a two-stream mixing layer. Ph.D. thesis, Dept. Nuclear Engineering, University of Illinois.

SUNYACH, M. & MATHIEU, J. 1969 Zone de melange d'un jet plan. *Int. J. Heat Mass Transfer* **12**, 1679.

TOWNSEND, A. A. 1976 *The Structure of Turbulent Shear Flow*, 2nd edn. Cambridge University Press.

WYGNANSKI, I. & FIEDLER, H. E. 1970 The two-dimensional mixing region. *J. Fluid Mech.* **41**, 327.